A TRUNCATION ERROR MODEL AND ITS APPLICATION TO THE ACCURACY ANALYSIS OF CONSTRAINT VIOLATIONS

S. Yoon*
Korean Institute of Aeronautical Technology, Seoul, Korea
and
R. M. Howe† and D. T. Greenwood‡
University of Michigan, Ann Arbor, Michigan

Abstract

Theoretical analyses for general Lagrange equations with algebraic constraint equations show that constraint equations should be differentiated twice, in general, for the whole system to be solved numerically without iteration. Then the original constraint equations are rapidly violated, since the differentiated constraint equations are unstable and numerical errors during computation continuously disturb the system. Baumgarte's modified form of second-order differential constraint equations was suggested to resolve this problem. A study is made of truncation errors and their modeling in the continuous time domain. This model can be used to determine the effectiveness of various constraint controls, including Baumgarte's, and integration methods in reducing the errors in the solution due to truncation errors. The extended model of truncation errors makes the accuracy analysis of constraint errors possible in a simple case, where Baumgarte's constraint control is applied.

Introduction

Theoretical analyses[1-3] for general Lagrange equations with algebraic constraint equations show that constraint equations should be differentiated twice, in general, for the whole system to be solved numerically without iteration. The differentiation of constraint equations was shown to result in unstable numerical solutions. This problem was seemingly resolved by Baumgarte's Constraint Violation Stabilization Method (CVSM)[4].

In this paper the accuracy of Baumgarte's CVSM is analyzed. For the purpose constrained dynamic systems are first defined along with the introduction of Baumgarte's CVSM. Energy constraint control[4-6] will be reviewed briefly for later use in the accuracy analysis. The truncation errors will be modeled in the continuous time domain to understand the relation between the accuracy of the simulated state variables and the constraint violations. The truncation error model will be used to determine the numerical disturbance which causes the constraint to be violated, and will be applied to a simple example in order to study the accuracy of the constraint errors.

Constrained Dynamic Systems

When the Lagrange multiplier method is applied to a dynamic system with holonomic constraints[7,8], the equations of motion are described by

$$M(q)\ddot{q} + \Phi_q^T\lambda = G(q,\dot{q},t) \tag{1}$$

$$\Phi(q,t) = 0 \tag{2}$$

where the holonomic constraint functions Φ: $R^{n+1} \rightarrow R^m$, generalized coordinates $q \in R^n$, $m < n$, and time $t \geq 0$. In Eq. (1), $\lambda \in R^m$ is a Lagrange multiplier. The inertia matrix $M \in R^{nxn}$ is positive definite, and $G \in R^n$ represents the remaining dynamic terms in the equation. Then the dynamic system with holonomic constraints is described by a set of n differential equations (1) and m algebraic equations (2).

If the Lagrange multiplier λ can be computed or expressed in terms of q, $\dot{q}$, and t, then the system of algebraic differential equations can be solved numerically. A fundamental method for computing λ without using implicit algorithms is to differentiate the constraint equation (2) twice with respect to time. This results in the equation

$$\ddot{\Phi}(q,\dot{q},\ddot{q},t) = 0 \tag{3}$$

Then the final equation for numerical computation has the form

$$\ddot{q} = A\left(q,\dot{q},\lambda(q,\dot{q},t),t\right) \tag{4}$$

Since the n second-order differential equations in q do not involve the m Lagrange multipliers λ in (4), the equations of motion can be solved numerically. In this paper, Eq. (4) is the differential equation that forms the basis for the numerical simulations.

Baumgarte's Constraint Violation Stabilization Method

A control $U(\Phi,\dot{\Phi},t)$ can be added to the right side of Eq. (3) in order to stabilize the reduction of the geometric constraint violations. Thus we let

$$\ddot{\Phi} = U\left(\Phi,\dot{\Phi},t\right) \tag{5}$$

where Baumgarte[4] suggests the form

$$U \equiv -\alpha\dot{\Phi} - \beta\Phi \tag{6}$$

Energy Constraint Control

If the total energy of a dynamic system can be computed from the initial energy plus the time integral of the energy input rate due to external or internal forces, then the total energy can be artificially treated as a constraint. This constraint is named an energy constraint, while conventional holonomic or nonholonomic constraints are defined as geometric constraints in this paper. It is a necessary condition for exact simulation that both geometric and energy constraints must be satisfied. When geometric constraint control is combined with energy constraint control, numerical simulation of a constrained dynamic system becomes more accurate[9].

There are at least two methods available in the literature for implementing an energy constraint, using the Lagrange equations of motion. The first method is described by

* Chief Research Engineer, Flight Simulation Team Memeber, AIAA
† Professor, Department of Aerospace Engineering Fellow, AIAA
‡ Professor, Department of Aerospace Engineering Associate Fellow, AIAA

Baumgarte[4]. The idea is to use the dynamic constraint equations modified from the original energy constraint equations in a manner similar to the nonholonomic case. If ψ is the energy constraint function, we let

$$\dot{\psi} + \eta\psi = 0, \qquad \psi = \psi(q,\dot{q}) \tag{7}$$

where η is a feedback gain constant. In general,

$$\psi \equiv T + V - (T + V)_0 - \int_{t_0}^{t} \dot{E}\, d\tau \tag{8}$$

where $\dot{E}$ is the energy input rate to the system. For a conservative system

$$\psi = E - E_0 \tag{9}$$

where E is the total energy, expressed in terms of q and $\dot{q}$.

The second method for implementing energy constraint control is based on the steepest descent algorithm[10]. The correction forces are applied to the equations of motion so that the integration of $\dot{q}$ and $\ddot{q}$ moves in the direction which most rapidly reduces the violation of the energy constraint[5,6]. To ensure that the minimum[6] of ψ is zero, the negative gradient of ψ^2 is fed back into the equations of motion (4). That is,

$$\frac{dq}{dt} = v - \rho_q \frac{\partial \psi^2}{\partial q}$$
$$\frac{dv}{dt} = A(q,v,t) - \rho_v \frac{\partial \psi^2}{\partial v} \tag{10}$$

Here ρ_q and ρ_v are positive gain constants to be determined and, ideally, $\psi(q,v) = 0$. Since $\partial\psi^2/\partial q = 2\psi(\partial\psi/\partial q)$ and $\partial\psi^2/\partial v = 2\psi(\partial\psi/\partial v)$, these control terms disappear when ψ=0. In the analytic solution, $\psi = 0$ is satisfied. Thus, implementation of the energy constraint control in (10) does not change exact solution of the original dynamic system equations. Both $\dot{q}$ and v can be considered to represent the total time derivative of q. However, d/dt is used to express the total time derivative when constraint control terms are added . The method in (10) of energy constraint control has been successfully applied in the computation of space and reentry trajectories[5]. Note that (10) is different from (7), and that (10) is simpler to implement.

Consideration of Truncation Errors

Consider the state equation dX/dt = F, and the Taylor series representation of X_{k+1} in terms of X_k and its derivatives:

$$X_{k+1} = (X_{k+1})_{Exact} = X_k + hF_k + \frac{h^2}{2}\dot{F}_k + \frac{h^3}{6}\ddot{F}_k + \ldots\ldots \tag{11}$$

where h is the integration step size. Integration algorithms can be considered as truncated Taylor series expansions. The Taylor series terms eliminated by the series truncation constitute the truncation error. Here we use Euler integration to illustrate the truncation error. Starting with the state X_k and state derivative F_k at t = kh, the Euler integration formula is simply

$$(X_{k+1})_{Euler} = X_k + h\,F_k \tag{12}$$

Thus, to order h^2, Euler integration is related to exact integration by the approximate formula

$$(X_{k+1})_{Euler} - (X_{k+1})_{Exact} \cong -\frac{h^2}{2}\dot{F}_k \tag{13}$$

In writing (13) we have assumed that $|h^3\ddot{F}_k|/6 << |h^2\dot{F}_k|/2$. If λ_x is the eigenvalue of a linearized version of the first-order differential equation, then $\ddot{F}_k = \lambda_x\dot{F}_k$, and it is clear that the approximation represented by (13) is equivalent to assuming $|\lambda_x h| << 1$. The truncation error $-(h^2/2)\dot{F}_k$ is called the local truncation error[11,12], since it is the truncation error introduced by the single integration step from time kh to (k+1)h. In general, the local truncation error for single-pass integration algorithms has the following form[12]:

$$(X_{k+1})_{Integ} - (X_{k+1})_{Exact} = -e_I h^{j+1}\left(\frac{d^jF}{dt^j}\right)_k \tag{14}$$

where e_I is a unique constant for each integration algorithm and j is the order of the integration algorithm. From Eq. (13) we see that $e_I = 1/2$ and j=1 for Euler integration. From the definition of integration we can write

$$(X_{k+1})_{Integ} - X_k = \int_{kh}^{(K+1)h} F\,dt \tag{15}$$

The area approximated by the numerical integration is equal to

$$(X_{k+1})_{Integ} - X_k = \int_{kh}^{(K+1)h}\left(\frac{dX}{dt}\right)_{Integ} dt \tag{16}$$

where $(dX/dt)_{Integ}$ is the approximation to $(dX/dt)_{Exact}$ which, when integrated exactly, generates the numerical approximation to the area in (16). Eq. (14) can be rewritten as

$$(X_{k+1})_{Integ} - (X_{k+1})_{Exact} \cong -h\left[e_I h^j\left(\frac{d^jF}{dt^j}\right)_k\right] \tag{17}$$

The right side of (17) represents the difference between the area under the dX/dt = F curve and the area approximated by the numerical integration. If h is small enough, d^jF/dt^j can be approximated as a constant over the interval [kh, (k+1)h]. Thus we can write

$$(X_{k+1})_{Integ} - (X_{k+1})_{Exact} \cong -\int_{kh}^{(k+1)h}\left[e_I h^j\left(\frac{d^jF}{dt^j}\right)_k\right]dt \tag{18}$$

Subtracting (15) from (16) and equating the integrand of the resulting expression to the integrand in (18), we obtain

$$\left(\frac{d}{dt}X\right)_{Integ} \cong F - e_I h^j \frac{d^j}{dt^j}F \tag{19}$$

It should be noted that the truncation error model in (19) assumes a single-pass integration algorithm[12]with $|\lambda_x h| << 1$.

In this paper, the equations of motion of a constrained dynamic system have the form of Eq. (4). The single second-order differential equation is simulated by numerical integration of the following two first-order differential equations:

$$\frac{d}{dt} q = v \tag{20.a}$$

$$\frac{d}{dt} v = A(q,v,t) \tag{20.b}$$

If the truncation errors are modeled as in (19), the effective equations of motion become

$$\frac{d}{dt} q \cong v - e_1 h^j \frac{d^j}{dt^j} v \tag{21.a}$$

$$\frac{d}{dt} v \cong A - e_1 h^j \frac{d^j}{dt^j} A \tag{21.b}$$

Note in Eq. (21.a) that dq/dt, i.e., $\dot{q}$, is no longer equal to v. The disturbing effect of the truncation errors in (21) must be reduced in order to obtain an improvement in accuracy of the numerical simulation. The assumptions necessary for the truncation error modeling method in (21) to be valid are summarized below:

Assumption

The effect of truncation errors on the state equation (20) can be interpreted in the continuous time domain in the form of (21), if the following conditions are met: (1) the integration method must be single pass, or have truncation errors equivalent to a single-pass method.; (2) For all eigenvalues λ of a linearized version of the state equations, $|\lambda h| << 1$, where h is the integration step size.

We assume that the disturbing effects of truncation errors are counteracted by constraint violation controls. Ideally, the constraint controls should produce corrections in the state-variable derivatives which are exactly opposite to the truncation error disturbances. In practice it is shown that this is not possible, although approximate cancellation of truncation errors through constraint controls can be achieved in some cases. The truncation errors in (21.a) cannot be directly counteracted by applying Baumgarte's geometric constraint control without energy constraint control in (10), which causes the velocity to be violated in the simulation of a constrained dynamic system. This, in turn, allows energy constraint violation. That is, simulated state variables of a constrained dynamic system satisfy the geometric constraint, not the energy constraint. This results in inaccurate state variable solutions. Thus the truncation error model in (21) explains why both geometric and energy constraint controls are necessary for accurate simulation. In any case, the truncation error model represented in (21) is a vital key in understanding the effectiveness of various constraint controls in improving simulation accuracy.

Steady-State Error Anaysis

In this section we accomplish quantitative evaluation of the steady-state constraint violation in an example by using the truncation-error modelling approach. We start with a simple first-order differential equation, and, for specific numerical integration algorithms, develop formulas for the first two terms in the truncation error model. These results can then be directly applied to a constrained dynamic system with CVSM plus the energy constraint control. The application of the improved truncation error model is illustrated with the following Problem 1, since Problem 1 is simple enough to yield analytic results for the steady-state constraint errors:

Problem 1 (Fig 1)

A unit mass moves with constant velocity along a unit circle in the XY-plane. There is no external force and m = 1. In terms of rectangular coordinates X and Y the holonomic constraint equation is

$$\Phi = \frac{1}{2}\left(X^2 + Y^2 - 1\right) = 0 \tag{22}$$

The equations of motion with the modified constraint equation are

$$\ddot{X} = -\frac{\dot{X}^2 + \dot{Y}^2 - U}{X^2 + Y^2} X \tag{23.a}$$

$$\ddot{Y} = -\frac{\dot{X}^2 + \dot{Y}^2 - U}{X^2 + Y^2} Y \tag{23.b}$$

where $U = \ddot{\Phi}$. This example is utilized in Baumgarte's paper[4] to show the validity of CVSM's. The initial conditions are

$$X(0)=1,\ Y(0)=0,\ \dot{X}=0,\ \dot{Y}=1 \tag{24}$$

This corresponds to counterclockwise motion with unit velocity around the unit circle in Fig 2. Accompanying time histories of the state variables are presented in Fig 2. As expected, X = cos t and Y = sin t.

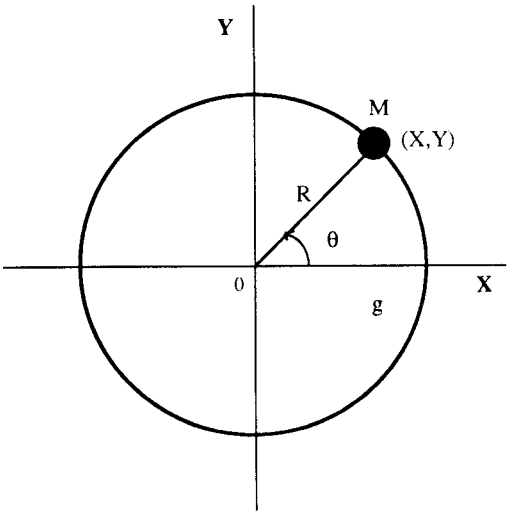

Fig 1. A unit mass rotating on a unit circle.

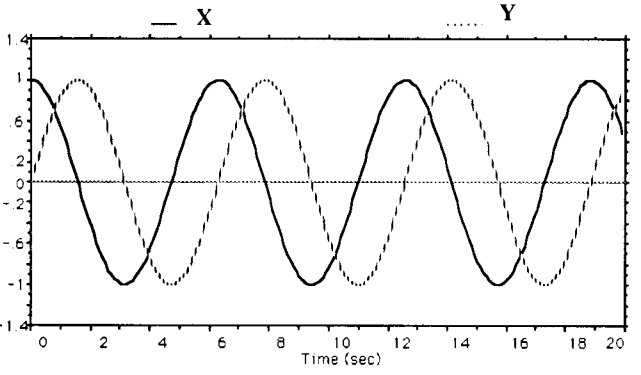

Fig 2. Problem 1 [X=cos t, Y=sin t] : Time histories of X and Y.

Consider the state equation $\dot{X} = F(X,t)$, and the Taylor series representation of X_{k+1} in terms of X_k and its derivatives:

$$X_{k+1} = X_k + hF_k + \frac{h^2}{2}\dot{F}_k + \frac{h^3}{6}\ddot{F}_k + \ldots. \tag{25}$$

Integration algorithms can be considered as approximations to the Taylor series expansion. For Euler integration the difference equation is

$$X_{k+1} = X_k + h\,F_k \tag{26}$$

Assuming X_k is exact, it follows that

$$\left(X_{k+1} - X_k\right)_{Euler} \cong \left(X_{k+1} - X_k\right)_{Exact} - \frac{h^2}{2}\dot{F}_k - \frac{h^3}{6}\ddot{F}_k \tag{27}$$

Taking the z-transform of (27) yields

$$(z-1)\hat{X}_{Euler} \cong (z-1)\hat{X}_{Exact} - \frac{h^2}{2}\dot{\hat{F}} - \frac{h^3}{6}\ddot{\hat{F}}$$

As before, we use "^" to denote z-transforms. In the case of sinusoidal inputs, i.e., $F = Ae^{j\omega t}$, we replace z by $e^{j\omega h}$ in the above z-transform[19]. In this case we also note that $\dot{\hat{F}} = j\omega\,\hat{F}$ and $\ddot{\hat{F}} = (j\omega)^2\hat{F}$. Making these substitutions, we obtain the following formula for the Euler integrator transfer function for sinusoidal inputs:

$$\frac{\hat{X}_{Euler}}{\hat{F}} \cong \frac{\hat{X}_{Exact}}{\hat{F}} + \frac{-j\frac{h^2\omega}{2} + \frac{h^3\omega^2}{6}}{e^{j\omega h} - 1} \qquad , \omega h << 1$$

We note that

$$\frac{\hat{X}_{Exact}}{\hat{F}} = \frac{1}{j\omega}$$

since an ideal integrator has the transfer function $1/j\omega$. Then it follows that

$$\left(\frac{\hat{X}_{Euler}}{\hat{F}}\right) \cong \frac{1}{j\omega} + \frac{-j\frac{\omega h^2}{2} + \frac{\omega^2 h^3}{6}}{j\omega h - \frac{1}{2}(\omega h)^2 - j\frac{1}{6}(\omega h)^3}$$

or

$$j\omega\,\hat{X}_{Euler} \cong \left[1 - \frac{h}{2}(j\omega) + \frac{h^2}{12}(j\omega)^2\right]\hat{F} \tag{28}$$

Recalling that $j\omega$ represents differentiation in the time domain, we can rewrite Eq. (28) as

$$\left(\frac{d}{dt}X\right)_{Euler} \cong F - \frac{h}{2}\frac{d}{dt}F + \frac{h^2}{12}\frac{d^2}{dt^2}F \tag{29}$$

For AB-2 integration, the difference equation is

$$X_{k+1} = X_k + \frac{h}{2}\left(3\,F_k - F_{k-1}\right) \tag{30}$$

Following the same procedure used to develop Eq. (29) for Euler integration, we obtain

$$\left(\frac{d}{dt}X\right)_{AB\text{-}2} \cong F - \frac{5h^2}{12}\frac{d^2}{dt^2}F + \frac{h^3}{4}\frac{d^3}{dt^3}F \tag{31}$$

The results in Eqs. (29) and (31) can be replaced by the following single truncation error model:

$$\frac{d}{dt}X \cong F + a_1 h\frac{d}{dt}F + a_2 h^2\frac{d^2}{dt^2}F + a_3 h^3\frac{d^3}{dt^3}F \tag{32}$$

where

$$a_1 = -\frac{1}{2}, \qquad a_2 = \frac{1}{12}$$

for Euler, and

$$a_1 = 0, \qquad a_2 = -\frac{5}{12}, \qquad a_3 = \frac{1}{4}$$

for AB-2. Note that the above results confirm the truncation error models developed previously, where we have included here an additional term in our error models.

For Problem 1, when the energy constraint control in Eq. (10) with $\rho_q = 0$ is combined with Baumgarte's CVSM, the state equations for X are

$$\frac{d}{dt}X = V_x \tag{33.a}$$

$$\frac{d}{dt}V_x = -X\frac{V_x^2 + V_y^2 - U}{X^2 + Y^2} - 2\rho_v\psi V_x \tag{33.b}$$

where

$$\Phi = \frac{1}{2}\left(X^2 + Y^2 - 1\right) \tag{34}$$

$$\psi = \frac{1}{2}\left(V_x^2 + V_y^2 - 1\right) \tag{35}$$

$$U = -\beta\,\Phi - \alpha\,\dot{\Phi} \tag{36}$$

$$\dot{\Phi} = X\,V_x + Y\,V_y \tag{37}$$

Note that $\dot{X}$ and $\dot{Y}$ are replaced by V_x and V_y, which represent the total time derivatives of X and Y, respectively. In this paper, d/dt is used to express the time derivative to be integrated numerically in the state equations. From (34) and (35), it follows that

$$X^2 + Y^2 = 1 + 2\,\Phi \tag{38}$$

$$V_x^2 + V_y^2 = 1 + 2\,\psi \tag{39}$$

Substituting (36), (38), and (39) into (33), we obtain

$$\frac{d}{dt}X = V_x \tag{40.a}$$

$$\frac{d}{dt}V_x = -X\frac{1 + 2\psi + \beta\Phi + \alpha\dot{\Phi}}{1 + 2\Phi} - 2\rho_v\psi V_x \tag{40.b}$$

We again note that the exact solution of Problem 1 with the initial conditions is given by X=cos t. In this case $\psi=\Phi=\dot{\Phi}=0$ in Eq. (40), which then becomes the differential equation for a linear oscillator with unit angular velocity. When (40) is integrated numerically, we can replace the time derivatives in (40) with the model given by Eq. (32). If the constraint violations are stable, then we expect Φ, $\dot{\Phi}$, and ψ to be nearly constant in the steady state. Thus we define

$$C \equiv \frac{1+2\psi+\beta\Phi+\alpha\dot{\Phi}}{1+2\Phi} \equiv \text{const} \tag{41}$$

The state equations in (40) can then be rewritten as

$$\frac{d}{dt}X = V_x \tag{42.a}$$

$$\frac{d}{dt}V_x = -CX - 2\rho_v \psi V_x \tag{42.b}$$

We now apply the numerical integrator model of (32) to (42) in order to obtain an equivalent continuous system. The result to order h^2 applies in the case of Euler integration and is given by

$$\frac{d}{dt}X = V_x + a_1 h \frac{d}{dt}V_x + a_2 h^2 \frac{d^2}{dt^2}V_x \tag{43.a}$$

$$\frac{d}{dt}V_x = -CX - 2\rho_v \psi V_x + a_1 h \frac{d}{dt}(-CX - 2\rho_v \psi V_x) \tag{43.b}$$

$$+a_2 h^2 \frac{d^2}{dt^2}(-CX - 2\rho_v \psi V_x)$$

Let us adopt the practice of choosing α and ρ_v to be proportional to h^{-1}, and choose β proportional to h^{-2}. Then it will be shown that the steady-state errors in Φ and ψ are of order h^2, and the steady-state error in $\dot{\Phi}$ is of order h. Also, $C = 1 + O(h^2)$. Thus, to zero order in h, the following equations apply when the Euler method is used to integrate (43):

$$\frac{d}{dt}V_x = -X$$

$$\frac{d^2}{dt^2}X = -X \tag{44}$$

$$\frac{d^2}{dt^2}V_x = -\frac{d}{dt}X$$

Also, $\rho_v\psi$ is of order h. Thus, Eq. (43.b) becomes, to order h^2,

$$\frac{d}{dt}V_x = (2a_1 h\rho_r\psi + a_2 h^2 C - C)X - 2\rho_r\psi V_x - a_1 hC\frac{d}{dt}X \tag{45}$$

From (43.a), to order h,

$$\frac{d}{dt}X = V_x + a_1 h \frac{d}{dt}V_x$$

which implies

$$V_x = \frac{d}{dt}X + a_1 h X \tag{46}$$

to order h. Using (46), we can rewrite Eq. (45) to order h^2, as

$$\frac{d}{dt}V_x = (a_2 h^2 C - C)X - (a_1 hC + 2\rho_r\psi)\frac{d}{dt}X \tag{47}$$

In Eq. (43.a), dV_x/dt and d^2V_x/dt^2 can be replaced by the representations in (44) and (47), respectively. Then (43.a) becomes, to order h^2,

$$\frac{d}{dt}X = V_x - a_1 hCX - (a_1^2 h^2 C + 2a_1 h\rho_r\psi + a_2 h^2)\frac{d}{dt}X \tag{48}$$

We now differentiate Eq. (48) and obtain, to order h^2, the following result:

$$\frac{d^2}{dt^2}X = \frac{d}{dt}V_x - a_1 hC\frac{d}{dt}X + (a_1^2 h^2 C + 2a_1 h\rho_r\psi + a_2 h^2)X \tag{49}$$

where d^2X/dt^2 on the right side has been replaced by $-X$ in accordance with (44). Substituting (47) into (49), we have finally

$$\frac{d^2}{dt^2}X + (2a_1 hC + 2\rho_r\psi)\frac{d}{dt}X + C(1 - a_2 h^2 - a_1^2 h^2)X \tag{50}$$

$$-(2a_1 h\rho_r\psi + a_2 h^2)X = 0$$

This is the modified differential equation in X when the Euler integration errors are considered to order h^2. Since zero damping occurs in the steady state,

$$2\,a_1 h\,C + 2\,\rho_v\,\psi = 0$$

From (41) it follows that

$$\psi = -\frac{a_1 h}{\rho_v}\left(\frac{1 + 2\,\psi + \beta\,\Phi + \alpha\,\dot{\Phi}}{1 + 2\,\Phi}\right) \tag{51}$$

From (50) the undamped natural frequency ω_n^* is given by

$$(\omega_n^*)^2 = -\rho_r\psi h\left(\frac{1}{a_1 h^2} - \frac{a_2}{a_1} + a_1\right) - a_2 h^2 \tag{52}$$

Another equation relating Φ, $\dot{\Phi}$, and ψ can be derived by establishing the expression for $\dot{\Phi}$. From (43.a)

$$V_x = \frac{d}{dt}X - a_1 h\frac{d}{dt}V_x - a_2 h^2\frac{d^2}{dt^2}V_x \tag{53}$$

From (45), to order h,

$$\frac{d}{dt}V_x = -CX - 2\rho_r\psi V_x - a_1 hC\frac{d}{dt}X \tag{54}$$

From (44), to zero order in h,

$$\frac{d^2}{dt^2}V_x = -\frac{d}{dt}X \tag{55}$$

Substituting (54) and (55) into (53), we obtain, to order h^2,

$$V_x = (1 + a_1^2 h^2 C + a_2 h^2)\frac{d}{dt}X + a_1 hCX + 2a_1 h\rho_r\psi V_x \tag{56}$$

Multiplying both sides of (56) by X, we obtain

$$XV_x = (1 + a_1^2 h^2 C + a_2 h^2)X\frac{d}{dt}X + a_1 hCX^2 + 2a_1 h\rho_r\psi XV_x \tag{57}$$

Similarly, for Y it follows that

$$YV_y = \left(1 + a_1^2 h^2 C + a_2 h^2\right) Y \frac{d}{dt} Y + a_1 h C Y^2 + 2 a_1 h \rho_r \psi Y V_y \quad (58)$$

In the steady state, we assume $\Phi = \Phi_{ss}$ = constant, and hence $d\Phi/dt = 0$. Thus we can write

$$X \frac{d}{dt} X + Y \frac{d}{dt} Y = \frac{d}{dt} \Phi = 0 \quad (59)$$

Since U is equal to $d^2\Phi/dt^2$, which is zero in the steady state, we obtain

$$U = -\alpha \dot{\Phi} - \beta \Phi = 0 \quad (60)$$

Eqs. (57) and (58) are added to obtain

$$\dot{\Phi} = XV_x + YV_y = a_1 h C\left(X^2 + Y^2\right) + 2 a_1 h \rho_r \psi \left(XV_x + YV_y\right)$$

From this equation and (60) it follows that

$$\dot{\Phi} = \frac{a_1 h}{1 - 2 a_1 h \rho_r \psi}\left(1 + 2\psi + \beta\Phi + \alpha\dot{\Phi}\right)$$

$$= \frac{a_1 h}{1 - 2 a_1 h \rho_r \psi}\left(1 + 2\psi\right) \quad (61)$$

We now have three equations, (51), (60), and (61), with the three unknowns Φ, $\dot{\Phi}$, and ψ. The steady state constraint violations can therefore be predicted to order h^2 using these equations. Using (60), we can simplify (51) to the following equation, to order h^2:

$$\psi \cong -\frac{a_1 h}{\rho_v} \quad (62)$$

In the same way, (61), to order h, becomes

$$\dot{\Phi} \cong a_1 h \quad (63)$$

Substituting (60) and (62) into (61) results in

$$\Phi = -\frac{\alpha}{\beta} a_1 h \left(1 - \frac{2}{\rho_v} a_1 h - 2 a_1^2 h^2\right) \quad (64)$$

If α, β, ρ_v, h and a_1 are given in the simulation, then ψ_{ss}, $\dot{\Phi}_{ss}$, and Φ_{ss} can be predicted from (62), (63), and (64), respectively. Note that ρ_V cannot be zero for ψ and Φ to be finite when a_1 is not equal to zero. This is in fact verified in the test simulations. We conclude for Problem 1 that the energy constraint control is essential in stabilizing the geometric constraint violation.

For second-order integration algorithms, the above analysis is not applicable, since a_1=0 in the second-order integration methods. For a second-order single-pass algorithm such as AB-2 the truncation error model represented in (32) can be applied to the state equations in (42) by including terms to order h^4. In this case we obtain, after some manipulations,

$$\Phi \cong \frac{\alpha}{\beta} a_3 h^3 \quad (65)$$

$$\dot{\Phi} \cong -a_3 h^3 \quad (66)$$

$$\psi \cong \frac{a_3 h^3}{\rho_v} \quad (67)$$

Eqs. (65), (66), and (67) can now be used to predict the steady-state errors in the constraints when using a second-order integration algorithm to solve Problem 1. Note that ρ_v is not involved in (65) for AB-2 integration, whereas it is in (64) for Euler integration. This relates to damping errors being dominant for odd integration methods, and frequency errors for even integration methods.

We now consider some test simulations for Problem 1 to compare predicted and actual steady-state errors in the constraints. The state equations used in the following examples are those represented by (62) through (67). The exact initial conditions of (5.1.16) are used in the simulations, i.e., X(0)=1, Y(0)=0, V_x(0)=0, and V_y(0)=1. In each of the following examples the integration method is stated, along with Baumgarte's gains (α, β), the energy control gain (ρ_v), the integration step size h, and the error coefficients in (32).

Example 1) Euler, α=200, β=10,000, ρ_v=5, h=0.01, a_1= −0.5. The simulation results for steady-state constraint errors are:

$\Phi_{ss} = 1.00200 \times 10^{-4}$
$\dot{\Phi}_{ss} = -5.01002 \times 10^{-3}$
$\psi_{ss} = 1.00180 \times 10^{-3}$

Eqs. (62), (63), and (64) predict

$(\Phi_{ss})_{pred} \cong 1.0 \times 10^{-4}$
$(\dot{\Phi}_{ss})_{pred} \cong -5.0 \times 10^{-3}$
$(\psi_{ss})_{pred} \cong 1.0 \times 10^{-3}$

Example 2) AB-2, α=(4/3)/h, β=(2/3)/h^2, ρ_v=0.5, h=0.01, a_3= 0.18. The simulation results for steady-state errors in the constraints are:

$\Phi_{ss} = 5.00039 \times 10^{-9}$
$\dot{\Phi}_{ss} = -2.50019 \times 10^{-7}$
$\psi_{ss} = 5.00038 \times 10^{-7}$

Eqs. (65), (66), and (67) predict

$(\Phi_{ss})_{pred} \cong 5.0 \times 10^{-9}$
$(\dot{\Phi}_{ss})_{pred} \cong -2.5 \times 10^{-7}$
$(\psi_{ss})_{pred} \cong 5.0 \times 10^{-7}$

These results demonstrate excellent agreement between simulated and predicted results, and confirm the validity of the truncation error model represented by Eq. (32).

Conclusions

The truncation error model in the continuous time domain allows interpretation of the relation between constraint violations and the accuracy of state variables. If the constraint control does not counteract the truncation error effects, then an accurate simulation may not be achieved, even if the geometric constraint violations are satisfactorily stabilized. The extended model of truncation errors makes the accuracy analysis of constraint errors possible in a simple case.

References

[1]Gear, C. W. and Petzold, L. R.,"ODE Methods for the Solution of Differential/Algebraic Systems," SIAM Journal of Numerical Analysis, Vol. 21, No. 4, 1984, pp. 716-721.

[2]Gear, C. W.,"Differential-Algebraic Equations," Computer Aided Analysis and Optimization of Mechanical System Dynamics, ed., E. J. Haug, NATO ASI Series, Series F, Vol. 9, Springer-Verlag, Heidelberg, 1984, pp. 316-334.

[3]Gear, C. W. and Leimkuhler, B.,"Automatic Integration of Euler-Lagrange Equations with Constraints," Journal of Computational and Applied Mathematics, Vol 12 & 13, 1985, pp. 77-90.

[4]Baumgarte, J.,"Stabilization of Constraints and Integrals of Motion in Dynamical Systems," Computer Methods in Applied Mechanics and Engineering, 1972, pp. 1-16.

[5]Fogarty, L. E. and Howe, R. M.,"Axis Systems for Analog and Digital Computation of Space and Reentry Trajectories," Application Report, Applied Dynamics, Inc., Ann Arbor, Michigan, September, 1963.

[6]Fogarty, L. E. and Howe, R. M.,"Space Trajectory Computations at The University of Michigan," Simulation, Vol. 6, No. 4, 1966, pp. 126-156.

[7]Greenwood, D. T., Principles of Dynamics, Prentice-Hall, 1988.

[8]Greenwood, D. T., Classical Dynamics, Prentice-Hall, 1977.

[9]Yoon, S.,"Real-Time Simulation of Constrained Dynamic Systems," Ph. D. Dissertation, Dept. of Aerospace Engineering, Univ. of Michigan, Aug.1990.

[10]Turner, R. M., "On the Reduction of Error in Certain Analog Computer Calculations by the Use of Constraint Equations," Proceedings SJCC San Francisco, 1960.

[11]Gear, C. W., Numerical Initial Value Problems in Ordinary Differential equations, Prentice-Hall, 1971.

[12]Howe, R. M., "Transfer Function and Characteristic Root Errors for Fixed-Step Integration Algorithms," Transactions of The Society for Computer Simulation, Vol. 2, No. 4, 1986, pp. 233-320.